A CELL MODEL FOR DUCTILE FRACTURE WITH APPLICATIONS TO THE TRANSITION REGIME

C. FONG SHIH, LI CHENG, JONAS FALESKOG and XIAOSHENG GAO
Division of Engineering Brown University
Providence, RI 02912 USA

ABSTRACT

A cell endowed with the micro-separation characteristics of the material is key to formulating a predictive tool for nonlinear fracture mechanics analysis. A cell should be viewed as a three-dimensional material unit, initially a cube with linear dimension D on a side, which contains a centered spherical void of initial volume fraction f_0; D is related to the microstructural length relevant to the tearing mechanism. Once the material-specific cell parameters have been calibrated by one set of experimental data, a computational model based on an aggregate of cells can compute relationships among load, displacement and crack growth of a structural component with no restrictions on the extent of plastic deformation and crack advance.

The discrete, three-dimensional nature of a cell enables it to capture important features of interaction between the fracture process and the nearby mechanical state including single cavity-crack tip interaction. It is this highly nonlinear coupling between the fracture process zone (FPZ) and the background material which gives rise to the rich variations of observed fracture behavior.

The computational model has been applied to fracture specimen geometries known to give rise to significantly different crack tip constraints and crack growth resistance behaviors. The model has successfully predicted the details of the load, displacement and crack growth in these geometries including surface cracks in thick plates subjected to different states of bending and tension.

KEYWORDS

fracture, ductile fracture, cleavage, toughness, constraint, void growth, finite elements

INTRODUCTION — CELL MODEL FOR DUCTILE TEARING

There is a long history of efforts directed at developing predictive computational tools for nonlinear fracture analysis, Rousselier (1987), Bilby *et al.* (1992) and Brocks *et al.* (1995)

among others. A fairly extensive list of such studies can be found in Xia *et al.* (1995) and Gao *et al.* (1996a). What will be discussed here is an approach based on a computational cell model of the material and the calibration of the material-specific cell parameters.

To motivate the model, we consider a typical structural steel containing inclusions on two different size scales. The large inclusions, e.g. manganese sulphides, range in size from 1 to 5 microns and have mean spacings of approximately 100 microns. A second population of submicron-sized inclusions, e.g. carbides, are found within grains and at grain boundaries. At the microscale level, the creation of new surfaces ahead of a pre-existing macrocrack follows a multistep failure process involving several interacting, simultaneous mechanisms: a) nucleation of microvoids by fracture or decohesion of large inclusions, b) subsequent growth of the larger microvoids, c) localization of plastic flow between the enlarged voids and d) the final tearing of the ligaments between enlarged voids, assisted by the rapid growth and coalescence of secondary microvoids. Micrographs show these processes of void growth and coalescence are confined to a narrow zone ahead of the crack front having a thickness of no more than a few hundred microns.

The above failure mechanism suggests the use of a computational model illustrated in Fig. 1 (Xia and Shih, 1995). A key feature is the modeling of the material in front of the crack as a layer of void-containing cells. Each cell is a three-dimensional material element which is initially a cube with dimension D comparable to the spacing between "large inclusions". Each cube contains a spherical void of initial volume fraction f_0. For the most part, the Gurson relation can be used to describe the stress-strain behavior of a single void-containing cell element (Gurson, 1977). At the heart of Gurson's relation is the yield condition

$$\Phi(\sigma_e, \sigma_m) = \left(\frac{\sigma_e}{\bar{\sigma}}\right)^2 + 2q_1 f \cosh\left(\frac{3q_2\sigma_m}{2\bar{\sigma}}\right) - [1 + (q_1 f)^2] = 0. \tag{1}$$

Here σ_e is the macroscopic effective Mises stress formed using the Cauchy stress, σ_m is the macroscopic mean stress, $\bar{\sigma}$ is the current flow stress of the matrix, f is the current void volume fraction, and q_1 and q_2 are the adjustment factors introduced by Tvergaard to improve the accuracy of the model (see Tvergaard, 1990).

The void in a cell grows under increasing strain. Eventually the strain-hardening of the matrix is insufficient to compensate for the reduction in the cell ligament area caused by void growth. Under these conditions, the cell begins to lose stress carrying capacity. Shortly thereafter, microvoids nucleate from secondary inclusions bringing about the final coalescence of voids that allows the crack to advance across the cell.

WORK OF FRACTURE

There are cogent arguments for embedding a fracture process zone (FPZ) within the elastic-plastic continuum (see discussion by Broberg, 1995). In our model, a FPZ naturally forms ahead of the advancing crack tip. This zone of width D and length ℓ is operationally defined by the collection of cells in which the strain softening due to void growth cannot be compensated for by material strain hardening resulting in a loss of stress carrying capacity.

The fracture process must obey an energy balance and under small scale yielding conditions the balance relation is simply

$$\mathcal{G} = \Gamma \tag{2}$$

where $\mathcal{G}$ is the Griffith-Irwin energy release rate. Under steady-state growth conditions Γ can be partitioned into the work of the fracture process, Γ_0, and the plastic dissipation in

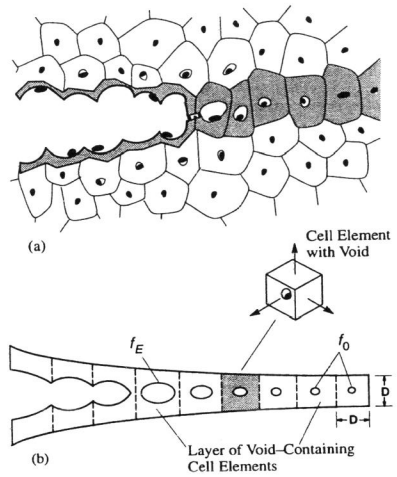

Fig. 1. (a) Void nucleation and growth creates a path of weak points in the material allowing macrocrack propagation by void coalescence; coalescence is assisted by microvoids nucleated from secondary inclusions. (b) Material in front of crack is modeled by cell elements of linear dimension D; each cell contains a single void of initial volume fraction f_0. Cell behavior depends on f_0 and tractions on all sides. The aggregate of cells is embedded within a conventional elastic-plastic continuum.

the background material, Γ_P, that is,

$$\Gamma = \Gamma_0 + \Gamma_P. \tag{3}$$

Actually some amount of residual elastic energy is locked in the remote wake and this has been included in Γ_P.

The work required to rupture a cell of unit area in the plane of the crack defines the work of the fracture process Γ_0 and this work depends weakly on constraint within the range found to exist near a crack tip (Xia and Shih, 1995b). For the first increment of crack growth, $\Gamma_0 \gg \Gamma_P$ so that $\mathcal{G} \approx \Gamma_0$. When crack extension is large compared to D and the material is very tough, $\Gamma_P \gg \Gamma_0$ with the result $\mathcal{G} \approx \Gamma_P$. The strong geometry dependence of experimentally measured resistance curves (the portion subsequent to initiation of growth) reflects the overwhelming contribution of Γ_P to the total work of fracture (cf. Hancock *et al.*, 1993, and Joyce and Link, 1995).

The above ideas are illustrated in Fig. 2; the plastic zone size, R_p, in the background material is not drawn to scale. Plastic dissipation in the background material (relative to Γ_0) is necessarily small when $\ell \approx R_p$ and must be large when $\ell \ll R_p$. Moreover, resistance curve characteristics can be explained in terms of the relative lengths ℓ/D and ℓ/R_p (Tvergaard and Hutchinson, 1992, 1994; Shih and Xia, 1995a, b).

MICROMECHANICS OF VOID COALESCENCE

Several mechanisms constitute the tearing process: nucleation of voids from the brittle cracking or decohesion of inclusions, growth of voids and, finally, void coalescence which

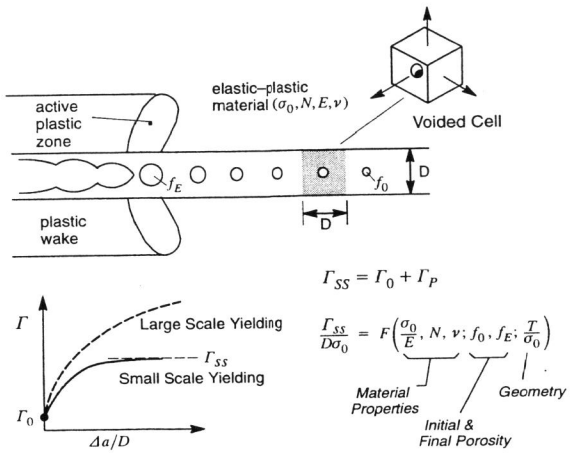

Fig. 2. Schematic illustration of steady-state growth. The fracture resistance depends on material-specific parameters and crack geometry. D enters explicitly as a scaling length for the steady-state toughness Γ_{SS}. The discrete, three-dimensional nature of a cell is highlighted. This enables it to capture important features of the coupling between between fracture process and plastic deformation in the background material including the strong triaxial stress effects on cavity growth and single cavity-crack tip interaction.

typically involves the participation of secondary microvoids. The mechanics of void growth is fairly well understood and models for this phase are quite advanced (see review article by Needleman *et al.*, 1992, and references therein). By contrast, coalescence micromechanics is less well understood and some aspects are discussed below.

Holes nucleate from (weak) large inclusions at relatively low stress. As these holes grow to large sizes under increasing stress a second population of small cavities nucleate from small inclusions residing primarily in the high stress and strain regions between the larger holes. The final tearing of the ligaments between larger voids is accomplished by the coalescence of rapidly growing microvoids. This mechanism of hole-joining involving the participation of small-scale voids along fairly narrow zones expends a small amount of energy compared to what is required for continued macrovoid growth. In any case, it is quite evident that the final outcome of this continuing competition — continued macrovoid growth vs. hole-joining assisted by microcavity nucleation — is determined by microstructure and carbide distribution as well as by external factors such as crack tip constraint.

For the materials in question, it appears that the underlying micromechanics of final ligament tearing is dominated the coalescence of rapidly growing microvoids originating from a population of small inclusions. Under high stress, a large void grows in concert with the plastic strain. Simultaneously, a local zone of high stress concentration emanates from the large void and spreads across the material raising the stresses at nearby microvoids. As a result, the hydrostatic stress surrounding one or more microvoids is raised to a level that activates an unstable deformation mode in which the stored elastic energy drives the plastic expansion of the microvoid. Although the overall stress decreases rapidly, small zones of high stress concentration are generated near growing voids — causing even smaller nearby

microvoids to grow rapidly. This process continues until the submicron ligament fails by microcleavage or by shearing along crystallographic planes.

Two mechanisms of material micro-separation — flat dimpled rupture and void-sheet formation — will now be discussed. Flat dimpled rupture is considered first. Figure 3(a) displays a typical stress-strain behavior of a representative material volume, viz. cell element, subjected to uniaxial straining. The response up to the peak stress is unexceptional. When microvoids are absent, the load in the post-peak stress regime drops gradually as shown by the dashed line. However, as can be seen the presence of microvoids results in a dramatic drop in the load. The accelerated load drop to point 'A' is the result of microvoid cavitation precipipating the final phase of the coalescence process shown in Fig. 3(b). Here, the largest microvoids have enlarged their volumes by more than three orders of magnitude and the plastic strain has localized within a narrow band on the order of the void size. At the same time, the growth rate of the large void has been substantially decreased because of the reductions in the macroscopic stress.

We now turn our attention to the coalescence by void-sheet formation between sulphide-nucleated voids (Cox and Low, 1974). Figure 3(c) shows a typical stress-strain behavior computed for a representative material volume strained under low constraint. Here, the relative peak stress is considerably lower than for the previous case. The macroscopic stress in the post-peak stress regime falls off smoothly when microvoids are absent. When microvoids are present, the stress drops more rapidly. At an advanced state, indicated by 'B', the intense plastic shearing is confined to a narrow band width on the order of the size of the enlarged microvoids. Figure 3(d) shows the band, joining large sulphide-nucleated voids, being populated by cavitated microvoids. The growth rate of the large voids has been greatly reduced while the microvoids aligned along the diagonal, and driven by evolving high local stresses, have enlarged by more than two orders of magnitude.

The highly coupled nature of the processes leading to final coalescence appears to be central to explaining both coalescence modes depicted in Fig. 3. The understanding gained from studies of coalescence micromechanics will be valuable to the present work in two ways: implementing a coalescence criterion and calibrating the cell response in the final coalescence phase.

CELL MODEL CALIBRATION

Before the computational model suggested in Fig. 1(b) and illustrated in Fig. 2 can be put to use, it is necessary to calibrate the material-specific cell parameters: the micromechanics parameters q_1 and q_2 and the fracture process parameters D and f_0.

Figure 4 contains an outline of the two-step calibration of the micromechanics and fracture-process parameters. The parameters characterizing the continuum plasticity properties, such as the yield strength and strain hardening are chosen to fit the true stress-strain curve for the material.

The micromechanics calibration is performed in two stages: First, the q_1 and q_2 parameters in the Gurson-Tvergaard (GT) constitutive equation are chosen by requiring the stress-strain behavior of the GT cell element to match the computed 3-D solution for the growth of a spherical void in a representative material volume (RMV) taking into account the strength and hardening characteristics of the matrix material. Details of the hole-growth mechanics calibration are provided elsewhere (Faleskog *et al.*, 1996). Next, the cell traction vs. cell elongation in the post-peak-stress regime is calibrated by means of a

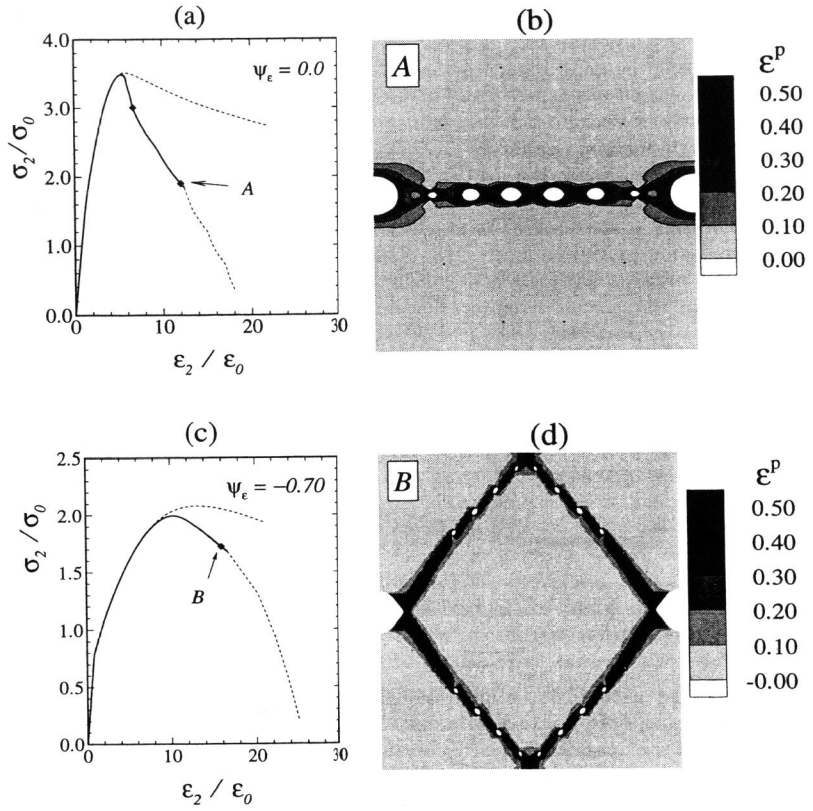

Fig. 3. Flat dimple rupture mode of coalescence under high strain biaxiality in a medium strength alloy ($\sigma_0/E = 0.002$, $N = 0.1$): (a) macroscopic stress-strain behavior featuring cascading softening, (b) advanced coalescence state at load point A, displaying contours of effective plastic strain.
Void-sheet mode of coalescence under low strain biaxiality in a high strength alloy ($\sigma_0/E = 0.004$, $N = 0.025$): (c) macroscopic stress-strain behavior, (d) advanced coalescence state at load point B, displaying contours of effective plastic strain.
Comment: An actual alloy will contain many more size scales of inclusions than have been considered above. Now, imagine that additional microvoids of even smaller size scale are found in the vicinity of the coalescence band. These minute microvoids embedded in a highly softened zone will in turn cavitate repeating the sequence in (b) and (d). This pattern of voiding gives rise to cascading load drops, indicated by dashes in (a) and (b), which repeat itself until finally the submicron ligament fails by microcleavage or shearing along crystallographic planes.

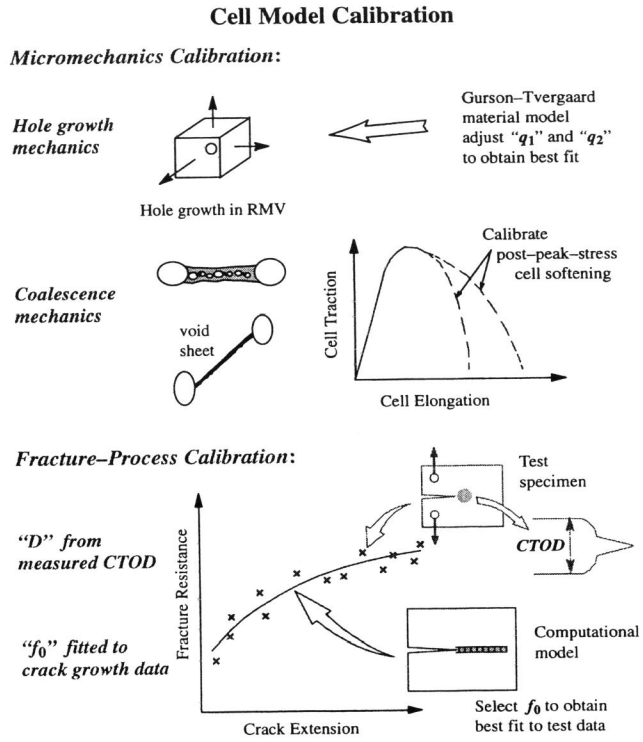

Fig. 4. Two-step calibration of cell model: (i) the micromechanics calibration uses a representative material volume (RMV), (ii) the subsequent fracture-process calibration requires a computational model of the reference test specimen used to generate the fracture resistance data.

micromechanics analysis of the type discussed in the preceding section.

Experimentally generated crack growth data are required to calibrate the two fracture-process parameters D and f_0. From the correlation of crack tip opening with the spacing of large inclusions it is reasonable to take D to be the measured crack tip opening displacement at fracture initiation ($CTOD_I$) (Xia and Shih, 1995). The remaining parameter, f_0, is chosen to give a best fit to a plot of the experimental fracture resistance vs. crack extension for one test. The fitting process entails several finite element crack growth analyses of that reference test specimen, using different values of f_0. A fair estimate of f_0 can be obtained by using a 2–D plane-strain computation and test data from a side-grooved specimen. A better value of f_0 is found by fitting 3–D computational model predictions to fracture resistance data from a standard, ungrooved test specimen. (The latter f_0 is slightly smaller than the former).

Experience shows that once the cell parameters have been calibrated in the manner de-

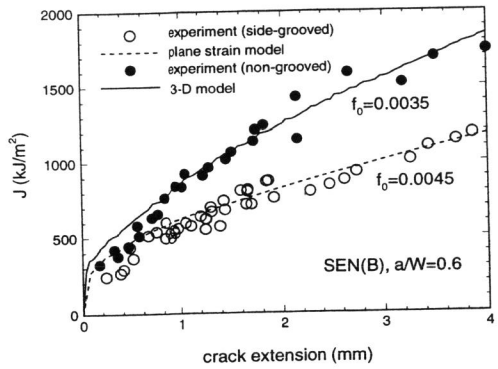

Fig. 5. Comparisons of measured fracture resistance for $2\frac{1}{4}$ Cr 1 Mo steel from side-grooved and ungrooved single-edged-notch bend specimens (crack length to width ratio, a/W, equal 0.6) with computed best-fits using plane strain and 3–D computational models. Note: $CTOD_I \approx J_{IC}/3\times$yield strength.

scribed, the computational model permits the accurate calculation of relationships among loads, displacements and crack growth, even for states where stability is lost. The computational model places no limit on the amount of crack advance nor on the extent of plastic deformation; moreover, once the model is calibrated no additional information is required for the the application of this approach to the calculation of the fracture resistance of structural components subjected to a wide variety of loadings, and having a range of initial crack shapes and sizes.

CALIBRATION AND VERIFICATION OF A PRESSURE VESSEL STEEL

The calibration scheme described above has been applied to a $2\frac{1}{4}$ Cr 1 Mo steel taken from a 20-year-old hydrogenating reactor pressure vessel. This a medium strength (yield strength = 255 MPa) high hardening ($N \approx 0.2$) material. The parameters characterizing the continuum plasticity properties, such as the yield strength and strain hardening, were chosen to fit the tensile stress-strain curve for the material. A micromechanics calibration of the material has been carried out by Faleskog *et al.* (1996); the hole-growth parameters are $q_1 = 2.0$ and $q_2 = 0.77$. For the fracture-process calibration we used experimental data from a single-edge-notch specimen loaded in bending, designated SEN(B). The $CTOD$ at fracture initiation was measured to be 300 microns — this value was assigned to D. The fitting of the crack growth data from side-grooved and non-grooved SEN(B) specimens is displayed in Fig. 5. An estimate of f_0 based on a plane-strain computational model is 0.0045. The better value, $f_0 = 0.0035$, was obtained from the 3–D computational model; this value was employed in subsequent applications. Figure 6 shows fracture surfaces of three specimens tested to increasing load levels (reading from right to left); measured crack profiles are compared with the corresponding model predictions. The agreement is remarkable! A detailed discussion of the above fracture-process calibration and verification is given by Gao *et al.* (1996b).

STRUCTURAL COMPONENT FRACTURE TESTS AND MODEL PREDICTIONS

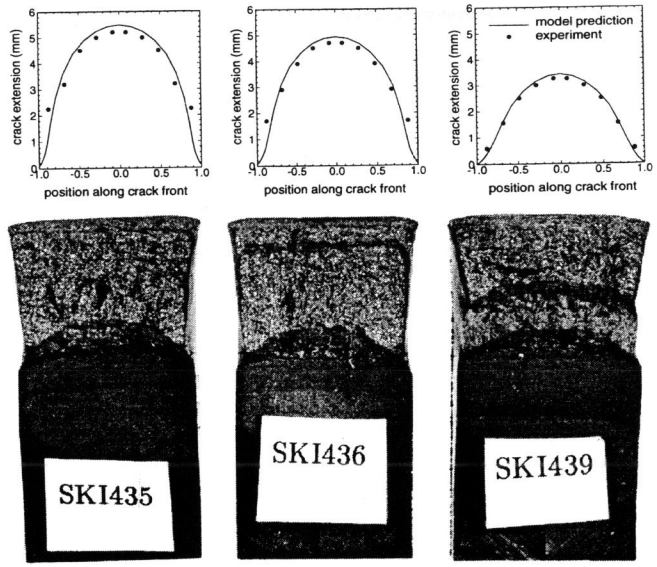

Fig. 6. Fracture surfaces of specimens broken apart after crack growth tests to different load levels (lowest load at right, highest at left). Comparisons of measured crack growth at various points along the specimen width with 3–D model predictions.

The predictive power of the computational approach based on a cell model of the material has been demonstrated in a laboratory setting. The application of this approach to the prediction of the behavior of structural components containing 3–D flaws is shown in Figs. 7 and 8. Thick plate specimens were fabricated from the $2\frac{1}{4}$ Cr 1 Mo steel. A surface crack was machined into the slightly curved thick plate designed to support different states of bending and tension. The finite element model of a quarter of the plate geometry displaying the crack plane and closeup views of the cell elements are shown in Fig. 7. A cell element has area $D/2 \times D/2$ in the plane whose normal coincides with the tangent to the crack front. The calculations were performed with WARP3D a research finite element code developed to handle large-scale models of 3–D solids. We use the measured true stress-strain curve, $q_1 = 2.0$ and $q_2 = 0.77$, and $D = 300\mu$m and $f_0 = 0.0035$. Figure 8(a) compares the computed load-deformation relationships with the experimentally measured behavior for two different tests. Figure 8(b) compares the measured crack growth at different points along the surface flaw from test SCT#9 (this specimen has a larger bending component) for two load levels with the predicted crack growth. It can be seen that the computational model has reproduced accurately the full details of the load-deformation curves and the crack growth profiles of both structural components. The detailed comparisons are described elsewhere (Gao *et al.*, 1996c). More experimental and computational studies are required to validate the cell model as an predictive tool for nonlinear fracture mechanics analysis. Nevertheless, we believe that the present results, when taken together with earlier studies based on the local fracture approach (Xia *et al.*, 1995, Gao *et al.*, 1996b,c, Ruggieri *et al.*, 1996 and references therein), provides a convincing case for the predictive power of computational approaches based on a cell model of the material.

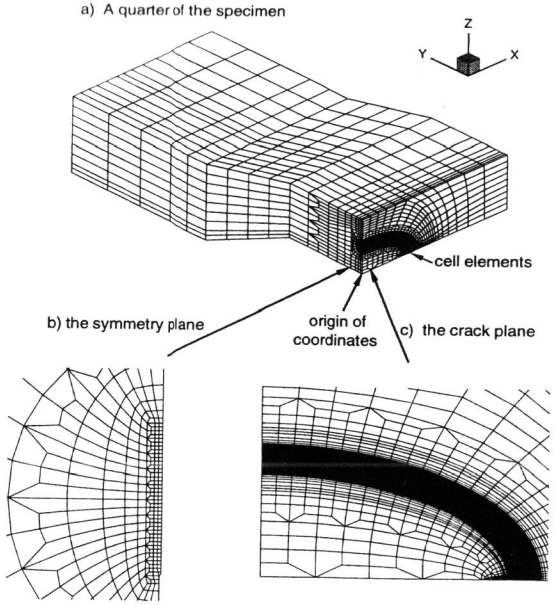

Fig. 7. Computational model of a slightly curved thick plate containing a part-through crack displaying cell elements. (a) finite element mesh of a quarter of the plate. (b) closeup of the $y - z$ plane of symmetry. (c) closeup of the $x - z$ plane of the crack. The geometry allows different combinations of tension and bending to be applied.

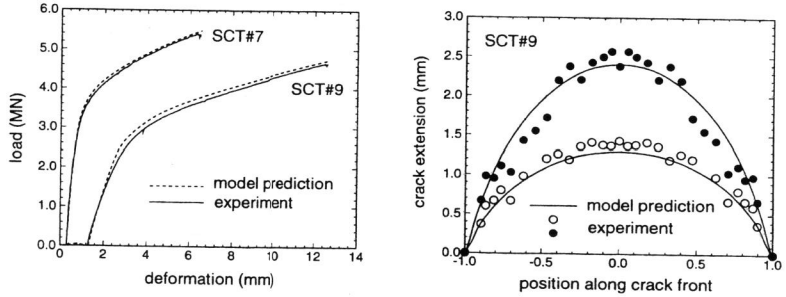

Fig. 8. (a). Comparisons of experimentally measured load vs. displacement for two different loading states with model predictions (SCT#9 has a higher bending load). Analyses use fracture-process parameters calibrated from the SEN(B) specimen ($D = 300$ microns, $f_0 = 0.0035$). (b) Comparisons of measured crack growth at various points along the part-through crack for two different load levels with predicted crack growth ($D = 300$ microns, $f_0 = 0.0035$).

Applications to fracture in the ductile/brittle regime

Two effects are associated with ductile crack growth: the cumulative sampling volume is increased and the crack tip constraint is altered. There are a fair amount of computational results documenting constraint elevation with crack growth in rate-independent and rate-independent solids (see Xia and Shih, 1995b, 1996, Gao *et al.*, 1996a, Varias and Shih, 1993, Xia and Cheng, 1996, and references therein).

Treatment of the initiation of unstable cleavage fracture by way of extreme value statistics has been discussed by Beremin (1983), Mudry (1987), Wang (1991), Wallin (1993) among others (see references therein). In these studies a weakest link mechanism is assumed for cleavage fracture. That is to say, at some point during the loading a microcrack nucleates at a critical second phase inclusion and this event is sufficient to precipitate catastrophic cleavage fracture. This approach has been extended by Koers *et al.* (1995), Xia and Shih (1996) and Ruggieri and Dodds (1996) to take account of the ductile crack growth prior to cleavage fracture. As in the Beremin model, the cumulative probability of unstable cleavage fracture can be phrased in terms of a critical value of the Weibull stress, σ_W, which scales with the product *stress* $\times$ *volume*. In several applications, the cell model for ductile tearing, incorporating weakest link statistics, predicts the change to cleavage fracture mode which is in agreement with experimental observations.

ACKNOWLEDGEMENTS

This investigation is supported by Grants N00167-K-0038 and N61533-93-K-0030 from David Taylor Research and Development Center funded by the Nuclear Regulatory Commission and by Grant N00014-95-1-0399 funded by the Office of Naval Research.

REFERENCES

Beremin, F.M. (1983) A Local Criterion for Cleavage Fracture of a Nuclear Pressure Vessel Steel, *Metallurgical Transactions A*, **14A**, 2277-2287.

Bilby, B.A., Howard, I.C. and Li, Z.H. (1992) Prediction of the first spinning cylinder test using ductile damage theory. *Fatigue Fract. Engrg. Mat. Struct.*, **16**, 1-20.

Broberg, K.B. (1995) Critical Review of Some Methods in Nonlinear Fracture Mechanics. *Engineering Fracture Mechanics*, **50**, 157-164.

Brocks, W., Klingbeil, D., Küencke G. and Sun D.-Z. (1995) Applications of the Gurson Model to Ductile Tearing, in *Constraint Effects in Fracture, Theory and Applications, ASTM STP 1244,* American Society for Testing Materials, Philadelphia, 232-254.

Cox, T. B. and Low, J. R. Jr. (1974) An investigation of the plastic fracture of AISI 4340 and 18 Nickel–200 grade maraging steels. *Metallurgical Transactions*, **5**, 1457–1470.

Faleskog, J.P. and Shih, C.F. (1995) Micromechanics of Coalescence - I. Synergistic Effects of Elasticity, Plastic Yielding and Multi-Size-Scale Voids. *J. Mech. Phys. Solids.* To appear.

Faleskog, J., Gao X. and Shih, C.F. (1996) Cell Model for Nonlinear Fracture Analysis — Micromechanics Calibration. Manuscript in preparation.

Gao, X., Shih, C.F., Tvergaard, V. and Needleman, A. (1996a) Constraint Effects on the Ductile-Brittle Transition in Small Scale Yielding. *J. Mech. Phys. Solids*, **44**, 1255-1282.

Gao, X., Faleskog, J. and Shih, C.F. (1996b) Cell Model for Nonlinear Fracture Analysis — Fracture-Process Calibration and Verification. Manuscript in preparation.

Gao, X., Faleskog, J., Dodds, R.H. and Shih, C.F. (1996c) Ductile Tearing in Part-Through Cracks — Experiments and Cell-Model Predictions. Manuscript in preparation.

Gurson, A.L. (1977) Continuum Theory of Ductile Rupture by Void Nucleation and Growth: Part I - Yield Criteria and Flow Rules for Porous Ductile Media. *J. Engin. Mat. Tech.*, **99**, 2-15.

Hancock, J.W., Reuter, W.G. and Parks, D.M. (1993) Constraint and Toughness Parameterized by T. In *Constraint Effects in Fracture, ASTM STP 1171*, American Society for Testing and Materials, Philadelphia, 21-40.

Joyce, J. A. and Link, R. E. (1995) Effects of Constraint on Upper Shelf Fracture Toughness. *Fracture Mechanics: 26th Symposium, ASTM STP 1256* , American Society for Testing and Materials, Philadelphia.

Koers, R.W.J., Krom, A.H.M. and Bakker, A. (1995) Prediction of Cleavage Fracture in the Brittle to Ductile Transition Region of a Ferritic Steel, in *Constraint Effects in Fracture, Theory and Applications, ASTM STP 1244,* American Society for Testing and Materials, Philadephia, 191-208.

Mudry, F. (1987) A Local Approach to Cleavage Fracture. *Nuclear Engineering and Design*, **105**, 65-76.

Needleman, A., Tvergaard, V. and Hutchinson, J.W. (1992) Void Growth in Plastic Solids, in *Topics in Fracture and Fatigue*, Ed., A. S. Argon, Springer Verlag, New York.

Ruggieri, C. and Dodds R.H. (1996) A Transferability Model for Brittle Fracture including Constraint and Ductile Tearing Effects: A Probabilistic Approach. *Int. J. Fract.* To appear.

Ruggieri, C., Panontin T.L. and Dodds R.H. (1996) Numerical Modeling of Ductile Crack Growth in 3-D Using Computational Cell Elements. *Int. J. Fract.* To appear.

Rousselier, G. (1987) Ductile Fracture Models and Their Potential in Local Approach of Fracture. Nuclear Engineering and Design, **105**, 97-111.

Tvergaard, V. (1990) Material Failure by Void Growth to Coalescence. *Adv. Appl. Mech.*, **27**, 83-151.

Tvergaard, V. and Hutchinson, J.W. (1992) The Relation between Crack Growth Resistance and Fracture Process Parameters in Elastic-Plastic Solids. *J. Mech. Phys. Solids*, **40**, 1377-1397.

Tvergaard, V. and Hutchinson, J.W. (1994) Effect of T-Stress on Mode I Crack Growth Resistance in a Ductile Solid. *Int. J. Solids and Struct.*, **31**, 823-833.

Varias, A.G. and Shih, C.F. (1993) Quasi-Static Crack Advance Under A Range of Constraints — Steady-State Fields Based on a Characteristic Length. *J. Mech. Phys. Solids*, **41**, 835-861.

Wallin, K. (1993) Statistical Aspects of Constraint with Emphasis to Testing and Analysis of Laboratory Specimens in the Transition Region, *Constraint Effects in Fracture, ASTM STP 1171*, American Society for Testing and Materials, Philadephia, 264-288.

Wang, Y.Y. (1991) A Two-Parameter Characterization of Elastic-Plastic Crack-Tip and Applications to Cleavage Fracture, Ph. D. Thesis, Department of Mechanical Engineering, MIT.

Xia, L. and Shih, C.F. (1995a) Ductile Crack Growth - I. A Numerical Study Using Computational Cells with Microstructurally-Based Length Scales. *J. Mech. Phys. Solids*, **43**, 233-259.

Xia, L. and Shih, C.F. (1995b) Ductile Crack Growth - II. Void Nucleation and Geometry Effects on Macroscopic Fracture Behavior. *J. Mech. Phys. Solids*, **43**, 1953-1981.

Xia, L. and Shih, C.F. (1996) Ductile Crack Growth - III. Transition to Cleavage Fracture Incorporating Statistics. *J. Mech. Phys. Solids*, **44**, 603-639.

Xia, L. and Cheng, L. (1996) Quasi-Statically Steady Crack Growth in Rate-Dependent Solids — One-Parameter Fields Under Different Constraints. *Int. J. Fract.* To appear.

Xia, L., Shih, C.F. and Hutchinson, J.W. (1995) A Computational Approach to Ductile Crack Growth under Large Scale Yielding Conditions. *J. Mech. Phys. Solids*, **43**, 389-413.